Accepted Manuscript

A comparative study of thermal stability of TNT, RDX, CL20 and ANTA explosives using UV 266 nm-time resolved photoacoustic pyrolysis technique

K.S. Rao, D. Ganesh, F. Yehya, A.K. Chaudhary

PII:	S1386-1425(18)31073-4
DOI:	https://doi.org/10.1016/j.saa.2018.12.011
Reference:	SAA 16640
To appear in:	*Spectrochimica Acta Part A: Molecular and Biomolecular Spectroscopy*
Received date:	14 June 2018
Revised date:	11 November 2018
Accepted date:	5 December 2018

Please cite this article as: K.S. Rao, D. Ganesh, F. Yehya, A.K. Chaudhary , A comparative study of thermal stability of TNT, RDX, CL20 and ANTA explosives using UV 266 nm-time resolved photoacoustic pyrolysis technique. Saa (2018), https://doi.org/10.1016/j.saa.2018.12.011

A comparative study of thermal stability of TNT,RDX,CL20 and ANTA explosives using UV 266 nm-time resolved photoacoustic pyrolysis technique

K. S. Rao[1,2], D. Ganesh[1], F. Yehya[1,3] and A. K. Chaudhary[1,*],

[1] Advanced Center for Research in High Energy Materials (ACRHEM), University of Hyderabad. India-500046.

[2] Present address: The Guo China-US Photonics Laboratory, Changchun Institute of Optics, Fine Mechanics and Physics, Chinese Academy of Sciences, Changchun-130033, China.

[3]Department of Physics, Faculty of Education, Al-Baida University, Al-Baida-38018, Yemen

*E-mail: akcphys@gmail.com, anilphys@yahoo.com

Abstract: The paper reports the potential use of UV based pulsed photoacoustic spectroscopy to study the thermal stability of some well-known premier explosives such as TNT, RDX, CL20, and ANTA between 30 and 350 ^{o}C range. The thermal PA spectra of samples were recorded using fourth harmonic wavelength i.e. 266 nm of pulse duration 7 ns and repetition rate 10 Hz obtained from Q-switched Nd: YAG laser system. Under the influence of UV radiation, the explosive molecules in vapor phase follow the photodissociation process and converted into their byproducts such as NO, NO_2 and N_2O etc. due to $\pi^* \leftarrow n$ transitions, which are responsible for the generation resultant PA signal at 266 nm wavelength. The results obtained from PA spectra as a function of temperature are cross verified with Thermo gravimetric-differential thermal analysis (TG-DTA) to ascertain the thermal stability of these samples. The comparative PA spectra of samples were analyzed and shown the behavior of acoustic modes with respect to incident laser energy, and data acquisition time. Finally, the thermal quality factor "Q" is measured to test the stability of reported explosives.

Keywords: UV 266 nm, thermal stability, photoacoustic, TNT, RDX, CL20, ANTA

1. Introduction

Synthesis of novel energetic materials is highly requisite, as they are widely used in military and civilian applications such as explosives, rocket fuels and gun propellants [1-10]. Thus, the designing of an energetic molecule is envisaged based on the thermal stability, performance, high velocity of detonation, detonation pressure compared to the known standard energetic compounds [11]. The novel energetic compounds of different properties can be synthesized which includes: the easy and cost-efficient, eco-friendly nature, production of non-toxic and non-hygroscopic byproducts during detonation, stability for long-time storage, insensitivity for safe transportation and handling, high enthalpy of formation, density and better oxygen balance is used for complete combustion. Furthermore, effective application of thermally stable energetic materials to military and civilian use needs detailed investigation. The premier explosive molecules possess common nitro ($–NO_2$) group but its bonding link varies from sample to sample. The nitro group, attached to aromatic or aliphatic carbon is probably one of the most widely studied of the functional group and this part is used for 'explosophore' in many energetic materials [7]. The functional group which are rapidly converted into the gaseous products during detonation of the molecule are called explosophore [4]. The nitrogen and oxygen-bearing nitro, nitroso, nitramine, nitrate ester and azido moieties are the members of the explosophore group. The oxygen content in the explosophore group is used for the conversion of molecular backbone to gaseous byproducts NO_2, CO_2, CO, and H_2O. There are many improvised spectroscopic techniques available for the stand-off and near-field detection of different HEMs [12]. No single technique has been found to be capable of detecting (i) all the explosives explicitly (ii) obscured/hidden explosives. They are either time consuming or involve sophisticated equipment along with tedious data analysis [13-16]. There is a need for identifying the pros and cons of each

technique, therefore, a detailed study is required to investigate the new cross mechanism in a direct manner for achieving the optimum results.

The PAS has several added advantages over the conventional absorption spectroscopy such as the effect of reflection, transmission and scattering are totally overruled. As a result, the low absorption coefficient and opacity of the sample affects the transmitted signal but do not have any effect on PA signal. Therefore, it has tremendous applications in spectroscopy of solids, liquids, gasses, condensed matter, nanoparticles and semiconducting materials etc. [17-26]. The PA technique offers several advantages such as high sensitivity, selectivity, simplicity and compact size, fast time response, non-destructive detection [22, 27-32]. It is widely recognized for its excellent performance in trace gas detection from ppb to ppt level [33,34]. In our previous work we have demonstrated the thermal decomposition mechanism, stability, and efficiency as rocket fuel for some of newly synthesized high energy materials using pulsed photoacoustic technique using excitation wavelengths of UV 266 nm and visible 532 nm, between 30-350 ^{o}C range [1,35-38]. It is known that the PA signal generation mechanism varies as a function of excitation wavelength. In case of UV range, it is attributed to electronic transition, whereas in the mid-IR wavelengths, it is due to vibrational modes of molecules [37,39,40]. Recently, we have extended our study to recorded the time resolved PA spectra of dimethyl methylphosphorate (DMMP) between 50-180 ^{o} C temperature range using mid-IR source [40]. In this report, we have choosen the 2-methyl-1,3,5-trinitrobenzene (TNT), 1,3,5-Trinitroperhydro-1,3,5-triazine (RDX), Octahydro-1,3,4,7,8,10-hexanitro-5,2,6-(iminomethenimino)-1H-imidazo(4,5-b)pyrazine (CL20), and 3-Nitro-1H-1,2,4-triazol-5-amine ANTA, to demonstrate their thermal stability and decomposition mechanism using UV 266 nm wavelength, for the first time. These samples are well known nirorich energetic compounds and possess different numbers of C-NO_2 and N-NO_2 bonds. Their thermal stability were studied by several resarch groups by various techniques [41-45]. By

considereing that the HEMs molecules vapor and it's major by products have strong absorption at UV 266 nm wavelength [46]. Therefore, it is important to evaluate the potential use of pulsed PA technique for existing nitro rich energetic compounds contain C-NO_2 and N-NO_2 bonds. In the case of 266 nm wavelength, the absorptions mechanism allowed the $\pi \rightarrow \pi^*$, $n \rightarrow \sigma^*$ and $n \rightarrow \pi^*$ transitions. Commonly, due to strong absorption of 266 nm wavelength, the HEMs vapor follows the photodissociation process and converts into their byproducts due to $n \rightarrow \pi^*$ transitions [36,47-50].

In the present report, we have compared the results obtained from both techniques i.e. PA spectroscopy and thermogravimetric-differential thermal analysis (TG-DTA) to understand thermal decomposition mechanism of TNT, RDX, Cl20, and ANTA, respectively. The comparative PA spectra analysis were carried out at decomposition temperature of samples. The study reveals that the positions of the principal functional group -NO_2 in aromatic rings of compounds is a key factor in their thermal stability.

2. Experimental arrangement

Thermal PA spectra of reported explosive samples were recorded using laboratory designed acoustic filter type resonance PA cell of length (l) = 7.5 cm, radius (R) = 0.75 cm (as shown Fig. 1) [51]. The resonant cell, with higher Q-value works as an amplifier which needs a low concentration of gas for the trace level detection. In a cylindrical PA resonance cell, the three types of eigenmodes are excited i.e. longitudinal, azimuthal and radial modes. The noise generated at the cell windows due to the light source can be controlled by buffer volume known as acoustic filters. In the designed PA cell, these have a length of 2 cm and a diameter of 0.8 cm. These filters suppress the noise from outside the sample. Now the main cavity works as a resonator and it is acoustically isolated [52]. In the case of a longitudinal resonator, the buffer volume should have a $\lambda/4$ length, where λ is the wavelength of the sound wave [53]. In PA cell design, a buffer volume considered as an acoustic filter at each end of

resonator leading to suppress the external noises and attenuation in the PA cell windows. Absorption of the laser beam by PA cell windows generates acoustic waves at the same resonant frequency of the resonator. So, the optimum dimension of buffer volume must be selected to act as a damper at the resonant frequency. The generated acoustic resonant modes inside the cylindrical cells can calculated well known equations is shown in ref [29].

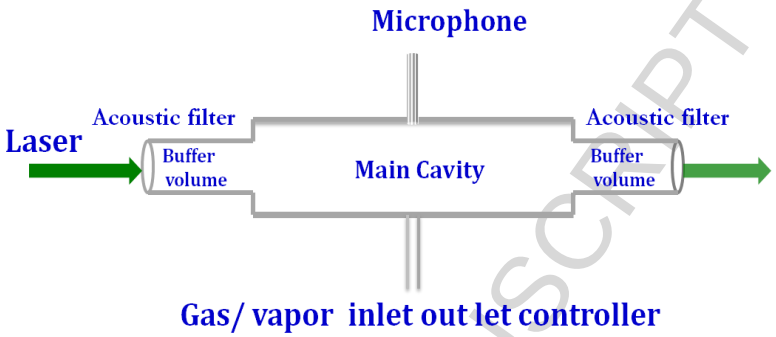

Fig.1 Designed PA cell.

It is observed that the PA spectra of explosives recorded using UV-266 nm radiations occupy frequency between 0-50 kHz range. The calculated acoustic frequencies of the given PA cell of length (l) =7.5 cm, radius (R) = 0.75 cm are listed in Table 1. The linear response of the detector microphone lies in between 0-60 kHz frequency range. In PA spectra of samples, the mixtures of the eigenmodes (i.e. acoustic frequencies) are strongly excited than the individual cavity modes. For this PA cell, the sixth and twelfth longitudinal modes are overlapped with first radial and azimuthal modes respectively. These modes are clearly observed and which are predominant in nature in PA spectra of reported samples.

Table 1: Calculated frequencies of PA cell (l=7.5 cm, R = 0.75 cm), at c= 343 m/s for dry air at 20 ^{o}C

Longitudinal (q) Modes f (kHz) (q) f (kHz)	1	2	3	4	5	6	7	8	9	10	11
	2.28	4.57	6.86	9.14	11.43	13.72	16.00	18.29	20.58	22.86	25.15
	12	13	14	15	16	17	18	19	20	21	22
	27.44	29.72	32.01	34.30	36.58	38.87	41.16	43.44	45.73	48.02	50.30
Radial (n) modes f (kHz)	1	2	3		*Azimuthal(m)modes f (kHz)*		1	2			
	13.4	22.2	30.5				27.89	38.8			

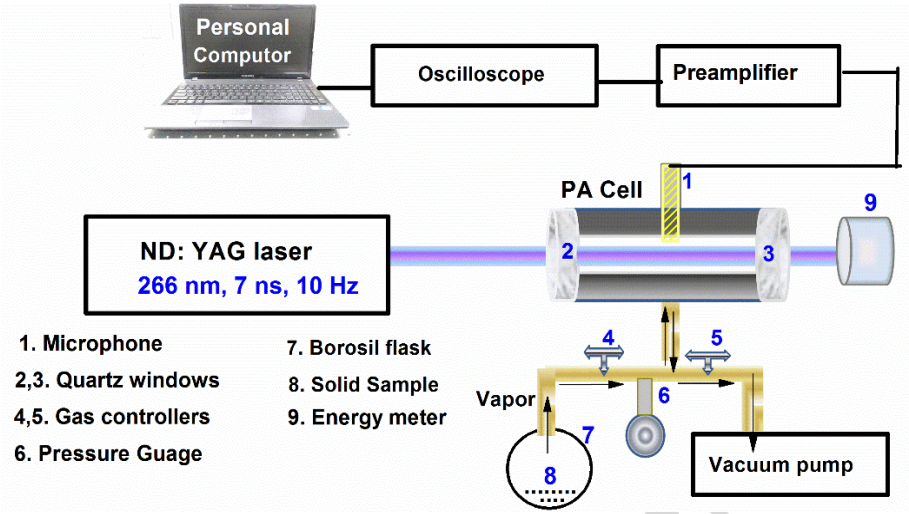

Fig. 2. Experimental setup.

Fig. 2 shows the experimental design used in our laboratory. A fourth harmonic wavelength i.e. 266 nm of pulse duration 7 ns and repetition rate 10 Hz obtained from Q-switched Nd: YAG laser (Model Spit, Germany) was used to excite the vapor of the explosives in an above mentioned cylindrical PA cavity. The laser beam diameter is adjusted to 6 mm using aperture and allowed to pass through the center of the PA cavity. The generated PA signal was detected by a pre-polarized microphone (housed in the center of a PA cell) of responsivity 50 mV/Pa (BSWA, China), and frequency range 0-60 kHz. The output signal of the microphone was fed to the preamplifier coupled to a 200 MHz oscilloscope (Tektronix, U.S.A.). The analysis was carried out using data acquisition program, which was developed using LabView software. The solid compound of a small quantity (~1 mg) is kept in a designed heating system, which facilitates the controlled pyrolysis between 30 and 350 ^{o}C range. The entire system was evacuated up to 10^{-2} Torr using a rotating vacuum pump. The released vapor of the explosive material at required temperature was introduced into the PA cell for the recording of PA spectrum at desired incident laser energy and data acquisition time. The input/output energies of exciting laser pulses were measured with a power meter (EPM2000, Coherent).

TG-DTA Instrument: Thermo gravimetric-differential thermal analysis (TG-DTA) was carried out using TA instrument (Model No. Q600DT). The solid compound was introduced into an alumina crucible and heated between ~30-500 ^{o}C range in a nitrogen atmosphere (flow rate of 100 cm^3 / min) which works as the purge and protective gas. An empty alumina crucible was used as a reference. Non-isothermal TGA runs were conducted between ~30-500 ^{o}C ranges at nitrogen atmosphere with purge rate of 10 ^{o}C/min. The thermogravimetric analysis provides the weight loss in the compounds, whereas DTA/ DSC provides the rate of heat flow as a function of temperature. Heat flow curve provides the information about melting, decomposition temperatures of the energetic materials. The compounds follow endothermic at their melting temperature and either exothermic or endothermic at decomposition temperature.

In addition, infrared spectra of solid samples were recorded using a Perkin- Elmer IR spectrometer between 400–4000 cm^{-1} range in form of KBr pellets.

3. Results and Discussions

3.1. FTIR spectra of samples

Before, recording the thermal PA spectra of reported explosives, it is important to identify the principle functional groups present in the samples. Therefore, the molecules were subjected to the FTIR spectra to record their structure in terms of vibrational frequencies due to the presence of principal functional groups. Fig. 3(a-d) shows the IR absorptions bands of TNT, RDX, CL20, and ANTA, respectively. These samples possess several vibrational frequencies between 1500-1300 cm^{-1} range and confirms the presence of $–NO_2$ group. Similarly, other absorption peaks between 3100-3000 cm^{-1} (C-H), 860-680 cm^{-1} (C-C), 1700-1500 (C=C) and 1250-1020 cm^{-1} (C-N) etc. are also present in all the samples. The additional absorption peaks of the amino group (in case of ANTA) are present at 3419.18, 3254.79 and 1649.32 cm^{-1}, respectively. Finally, the comparative FTIR spectra is shown in Fig.3 and confirm the

presence of different functional groups in the reported samples. Further, we have chosen these samples to record the PA spectra as a function of temperature to study their thermal stability and decomposition mechanism.

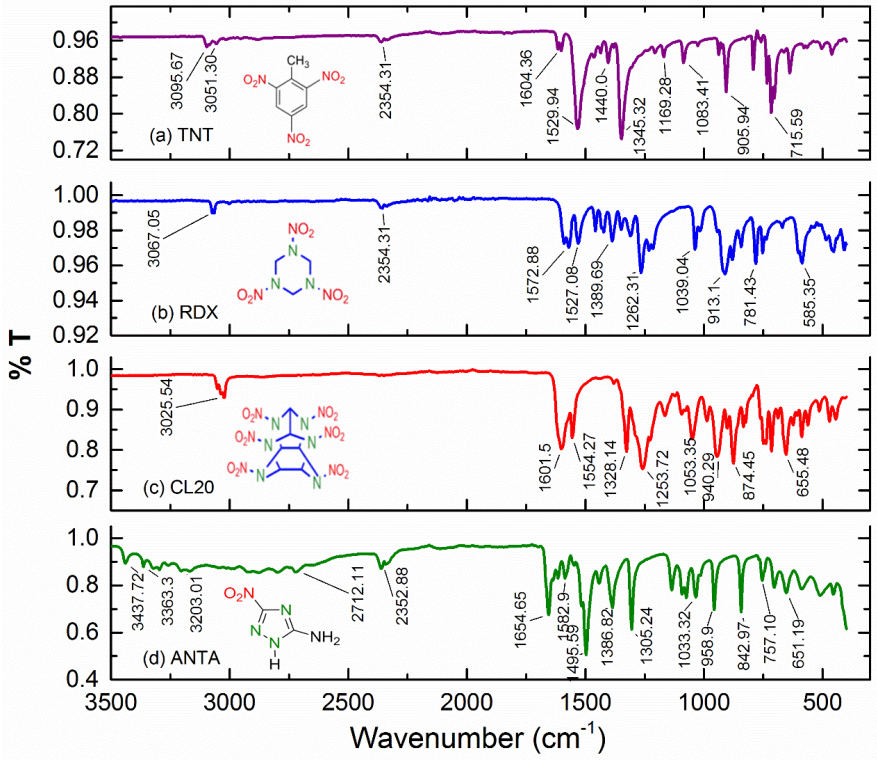

Fig. 3. FTIR spectra of samples.

3.2. Thermal PA spectra and TG-DTA analysis

Fig. 4(a-d) shows the thermal PA spectra of TNT, RDX, CL20, and ANTA, respectively at incident laser energy (E_{in}) =30 µJ and data acquisition time (t) =0.5 ms. The corresponding inset figures show the intensities of different acoustic modes as a function of temperature. Fig. 4(a) shows the thermal PA spectra of TNT, which has the excited acoustic modes 3.3, 8.6, 13.8 27.8 and 51 kHz, respectively. These acoustic modes show almost stable intensity up to 85 ^{o}C (T_m=81 ^{o}C), then after raise in their PA signal and possess peak at 150 and 300 ^{o}C, respectively. In the PA spectra of RDX (shown in Fig. 4(b)), the acoustic modes are located at 3.8, 8.6, 28.2, and 51.6 kHz shows the stable nature up to 150 ^{o}C, then there is an increment in their intensities with further growth in the vapor temperature. Similarly, the PA spectra of Cl20 (is shown in Fig. 4(c)), the acoustic modes present at 3.8, 8.4, 13.8, 28, and

38.8 kHz possess stable nature up to 200 ^{o}C and having highest intensity at 300 ^{o}C. The 220 ^{o}C, is close to its T_d and PA signal starts increasing at 240 ^{o}C (T_d). Similarly, for ANTA the excited acoustic modes are located at 3.8, 13.8, 28.0, 39.2, and 45.0 kHz shows it is thermally stable nature up to 250 ^{o}C. However, in case of different samples, due to contribution of total molecule vapor for the generation of PA signal, the excited acoustic modes almost possess similar frequencies with variation in their predominant order in the same PA cell. The excited acoustic modes have approximately similar values with the calculated eigenmodes of the given PA cell is listed in Table.1.

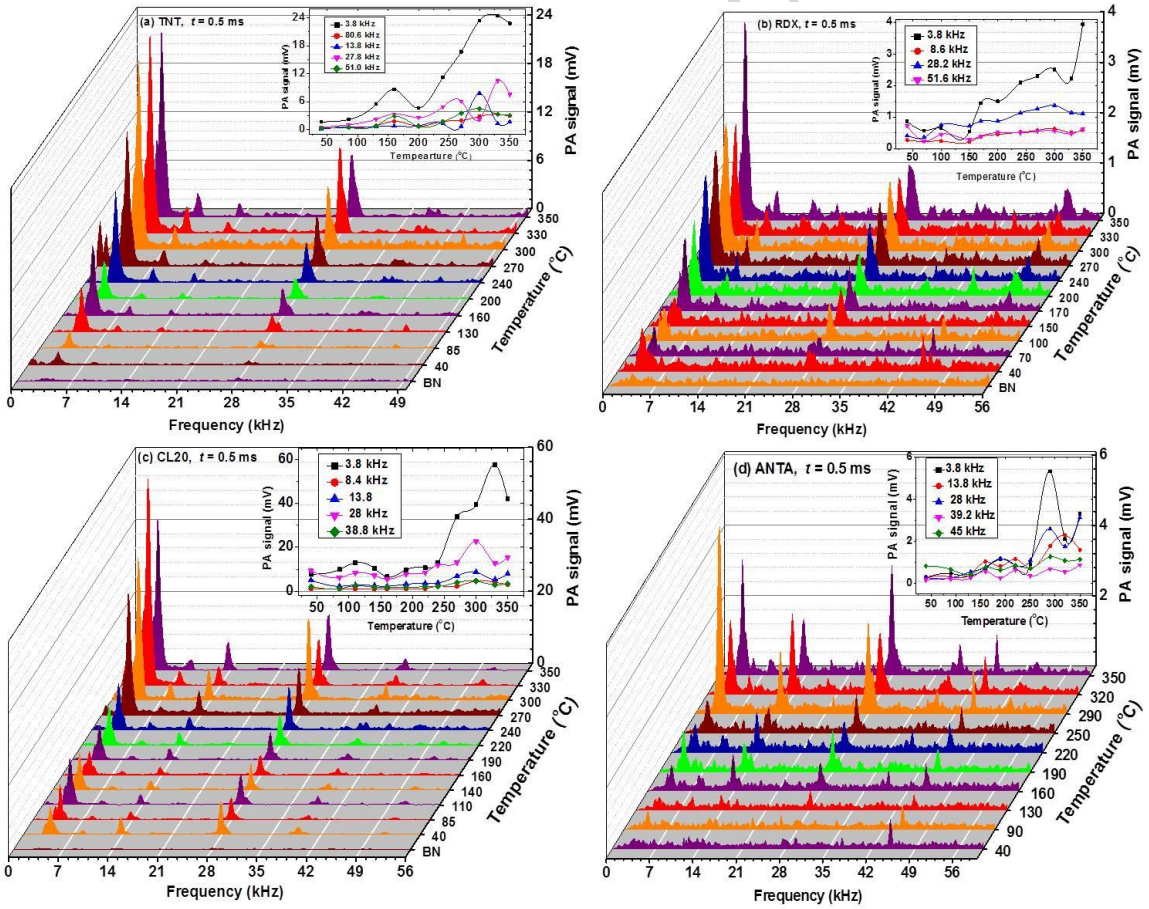

Fig. 4. PA spectra of samples and behavior of acoustic modes as a function of temperature.

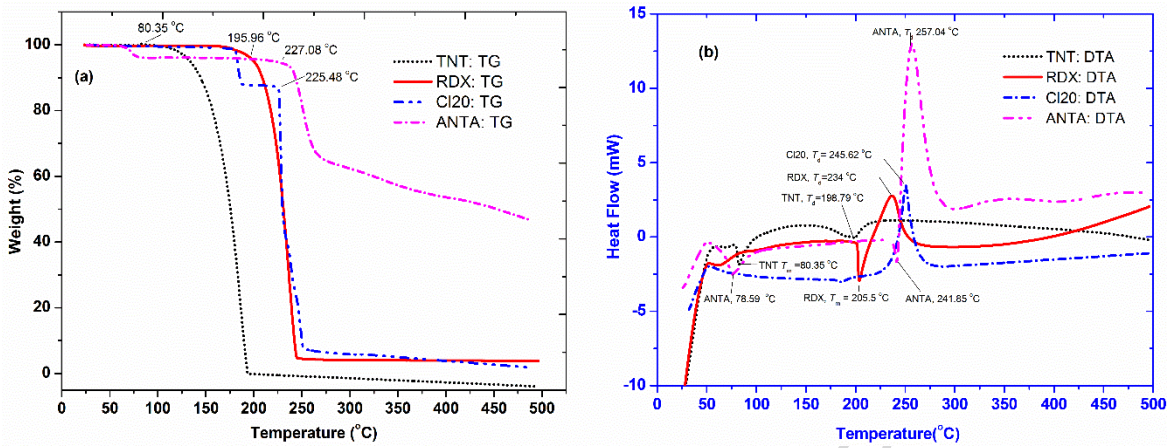

Fig. 5. TG-DTA analysis of samples corresponding to (a) Weight loss, and (b) Heat flow curves.

Table 2 Energetic properties of samples and the temperatures obtained from TG-DTA, and PAS (based on the higher strength of PA signal is achieved between 30-350 °C, range).

	Energetic properties		Thermal stability T(°C)		DTA		Highest PA signal achieved at T (°C)	Explosive property
Sample	ρ gm/cm^3	VOD km/s	From weight loss curves	From PA signal curves	T_m (°C)	T_d (°C)		
TNT	1.65	6.95	130	130	80.35	240	330	Melt castable
RDX	1.82	8.7	195.96	170	205.5	234	350	Thermally stable
CL20	2.04	9.4	225.98	240	245		300	High performance
ANTA	1.81	8.18	227.08	220	78.59	257.04	290	Thermally stable

Fig. 5(a,b) shows the TG-DTA curves of the samples. Fig. 5(a) exhibits the percentage weight loss of samples, which shows they initiate drastic weight loss at the corresponding temperatures 150, 195, 225, and 227 °C, respectively. Fig. 5(b) shows the heat flow curve indicating the melting (T_m) and decomposition (T_d) temperatures of the samples at heating rate 10 °C /min. The T_m and T_d of TNT is 80.35, 198.75 °C, RDX is 205.5, 234.0 °C and ANTA is 78.59, 257.04 °C, respectively. Whereas Cl20 has its common and T_m and T_d at 245.62 °C. The highest strength of the PA signal is achieved for the samples at their T_m, or T_d and after crossing the decomposition temperatures. In the present case, almost the samples possess the higher strength of PA signal after the decomposition temperature. At remaining temperature region the strength of PA signal possesses almost similar values which indicate

that the reported samples are thermally stable. The energetic properties such as density (ρ) and velocity of detonation (VOD) as well as the temperatures obtained from TG-DTA and PA spectra are comprised in Table. 2. In addition, we have performed the TG-DTA analysis with respect to the different heating rate of the samples. It was observed that the T_m and T_d values of these samples have a very slight variation with respect to different heating rates i.e. 5, 7.5, 10, and 12 ^oC/min. However, we have given the TG-DTA curves at the heating rate 10 ^oC/min is shown in Fig. 4.

From DTA analyis we directly measured the melting and decompostion tempeartures. However, we have correlate the thermal stabilty of samples based on the strength of PA signal as a function of temperature. Consequently, listed the tempearures based on

higher strength of PA signal among the 30-350 ^oC range in Table 2. It is obserevd that the strength of PA signal (insets of Fig. 4) as a function of tempearture shows similar up to centain tempearures (as mensioned above). Which indicates that up to these tempearture region, the compounds releases similar amount of gas mixture. In addition, the reported samples possess higher strength of PA signal after crossing the decomposition tempearture as compared to other temperatures. Thermally stable compounds releases equal or slightly higher quantity of gasesous mixures from one temperature to another, which reflects in PA signal intensities.

The compounds having a different number of nitro-groups. As we know that in case of 532 nm only NO_2 molecules (released from explosives during pyrolysis) are responsible for the generation of PA signal. At 266 nm the total molecule vapor is responsible for the generation of PA signal. However, the $–NO_2$ bonds are weak in nature compared to other bonds exit in reported samples. As a result, it is assumed to be the concentration of NO_2 molecules is high in the total molecule vapor. It was observed that highest intensity of PA

signal was achieved in case of CL20 due to its higher density (ρ=2.04 gm/cm^3) and VOD (9.4 km/s). The intensity order of PA signal for the samples follows CL20 > TNT > RDX > ANTA. The strength of PA signal, as well as TG-DTA, confirms the explosive properties of samples such as TNT is melt castable, RDX and ANTA are thermally stable, and CL20 is high performance explosive [7,54].

3.3. Comparative PA spectra of samples

Fig. 6(a-d) shows the PA fingerprint of TNT, RDX, CL20, and ANTA, respectively. The inset figures show the time domain signals. The PA spectra recorded at an incident laser energy (E_{in}) = 50 μJ and data acquisition time (t)=1.0 ms. The major excited acoustic modes and their corresponding intensities are shown in the Table. 3. The predominant order of acoustic modes varies from sample to sample. For all the four compounds the major two modes are present at 3.8 and 28 kHz, respectively, which have same values with the second longitudinal and first radial (as well as 12 longitudinal) modes, respectively. In case of ANTA, all the five modes are possessing comparable intensities. While for RDX and CL20 compounds only two modes i.e. 3.8 and 28 kHz having relatively higher intensities than the other modes. In case of TNT except for the 3.8 kHz, all other modes have similar intensity. The change in the intensities of acoustic modes clearly indicates that the variation of the acoustic signal with respect to different samples depends on their energetic properties.

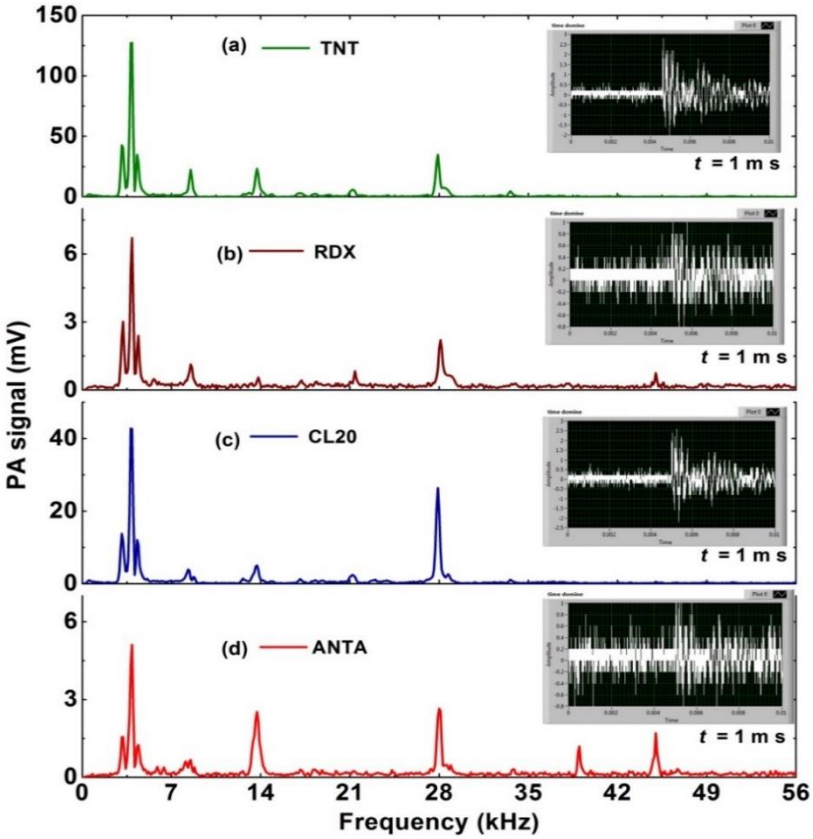

Fig. 6. Comparative PA spectra of samples.

Table. 3. Excited acoustic frequencies and their intensities at t=1 ms at T_d of the samples.

Sample	First line: frequencies (f) in kHz Second line: Intensity (I) in mV
TNT	f (kHz):3.1 3.9 4.3 8.5 13.7 21.2 27.9 33.7 I (mV):42.7 127.3 34.8 22.4 23.2 5.89 34.7 3.3
RDX	f (kHz): 3.2 3.9 4.4 8.5 13.8 17.2 21.4 28.1 45 I (mV): 3.1 6.7 2.4 1.1 0.6 0.4 0.8 2.2 0.8
Cl20	f (kHz): 3.1 3.9 4.3 8.2 13.7 17.2 21.2 27.9 33.5 I (mV): 13.8 42.6 12.1 2.8 5.1 0.9 2.45 23.4 0.8
ANTA	f (kHz): 3.2 3.9 4.4 8.1 8.5 28 45 I (mV): 1.6 5.1 1.3 0.6 0.7 2.7 0.7

3.4. The behavior of acoustic modes with respect to incident laser energy (E_{in})

Fig. 7(a-d) shows the PA spectra of explosives and inset figure shows the behavior of acoustic modes with respect to incident laser energy recorded at T=350 ^{o}C and t= 0.5 ms. The PA spectra of TNT is shown in Fig. 7(a) reveals that the excited acoustic modes possess exponential growth of PA signal. In case of 40 and 50 μJ PA spectra, the acoustic modes lie in the frequency range of 12-22 kHz have high intensity. For RDX is shown in Fig. 7(b), 3.8

kHz shows different nonlinear growth with incident laser energy while the other modes i.e. 8.6, 13.8 and 28.2 kHz are showing exponential growth in their intensity. In Fig. 7(c) for the compound CL20, the behavior of excited acoustic modes is different from one another with incident laser energy. This is attributed due to a higher concentration of released vapor (might be higher number of $–NO_2$ groups). Fig. 7(d) shows the PA spectra of ANTA, the intensities of acoustic modes increases simultaneously with further increase in the incident laser energy. The acoustic mode present at 28.2 kHz shows decrement after crossing 40 μJ energy. The acoustic modes at 13.8, 39 and 45 kHz show similar growth behavior. Even at 10 μJ, it is capable to record the PA spectra due to the high sensitivity of PA spectroscopy and the PA cell work as a resonator to amplify the PA signal. RDX and ANTA possess the similar strength of PA signal, even though at higher incident laser energies. At 50 μJ energy TNT possess the highest strength of PA signal compared to other three samples, while Cl20 possess higher intensities compared to RDX and ANTA. The behavior of acoustic modes in terms of their nonlinear growth reveals that the variation in the density of molecules vapor at given temperature. The variations in the laser energy lead to change the intensities of acoustic modes corresponding to their predominant order. However, the central frequencies of acoustic modes do not vary with respect to incident laser energy.

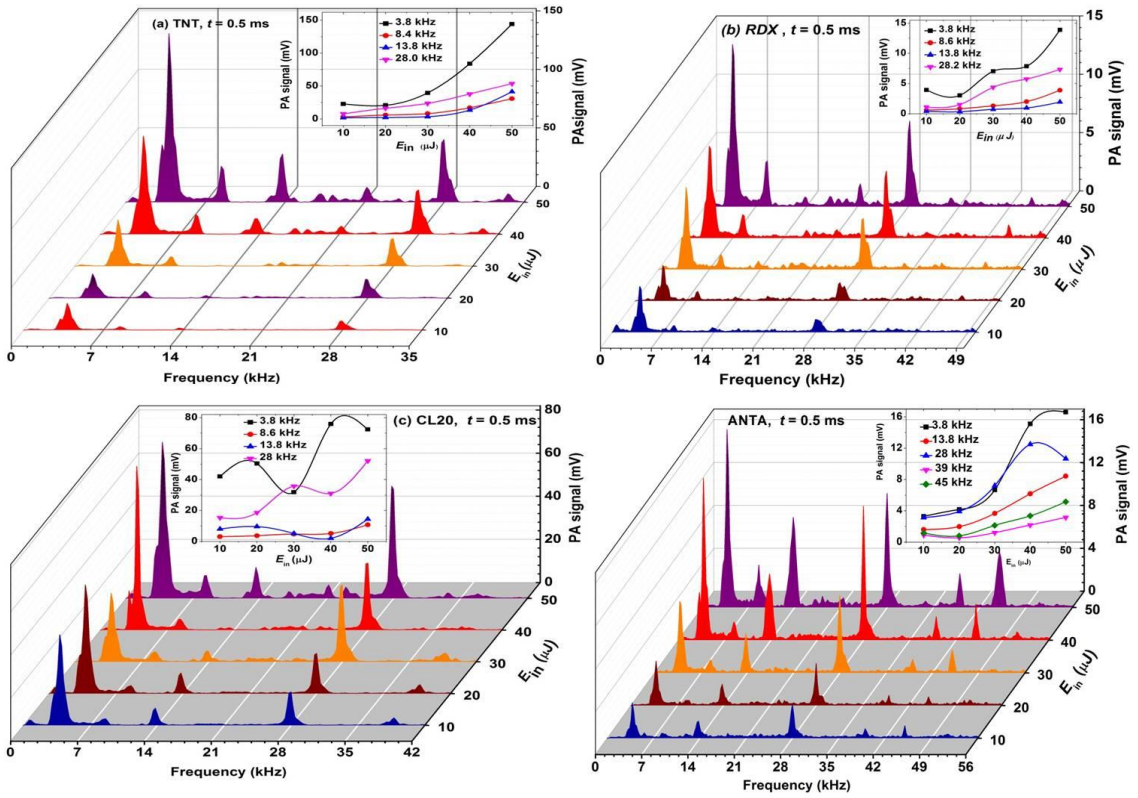

Fig. 7. PA spectra of samples with respect to incident laser energy (E_{in}).

3.5. The behavior of acoustic modes with respect to data acquisition time (*t*)

Fig. 8 shows the PA spectra of explosives and inset demonstrates the decay behavior of excited acoustic modes with respect to data acquisition time, respectively. The PA spectra are recorded at T_d of samples using incident laser energy 30 µJ. It is well known that the central frequencies of acoustic modes do not vary as a function of data acquisition time. The intensity of PA signal is inversely proportional to data acquisition time. To understand the tendency of acoustic modes in terms of their intensity, we have recorded the PA spectra at different timescales. All the acoustic modes show exponential decay behavior as a function of data acquisition time. Here, we are giving only the decay times of first predominant mode i.e. ~3.8 kHz for TNT, RDX, CL20, and ANTA are 0.42, 0.28, 0.41, and 0.93 ms, respectively. The modes which possess higher decay times indicates those are strong modes excited with different timescales. The samples possess at *t*= 2.5 ms almost negligible PA signal, however, for lower timescales, the intensity is significantly increased and the signal to noise ratio is comparatively high. This indicates that the compounds released a very lower

quantity of gaseous molecules, which directly shows the thermal stability of samples. The strength of PA signal for ANTA is very weak compared to other three samples. Even though there is a possibility to get the trace of PA signal due to high versatility and sensitivity of PA technique at UV wavelengths.

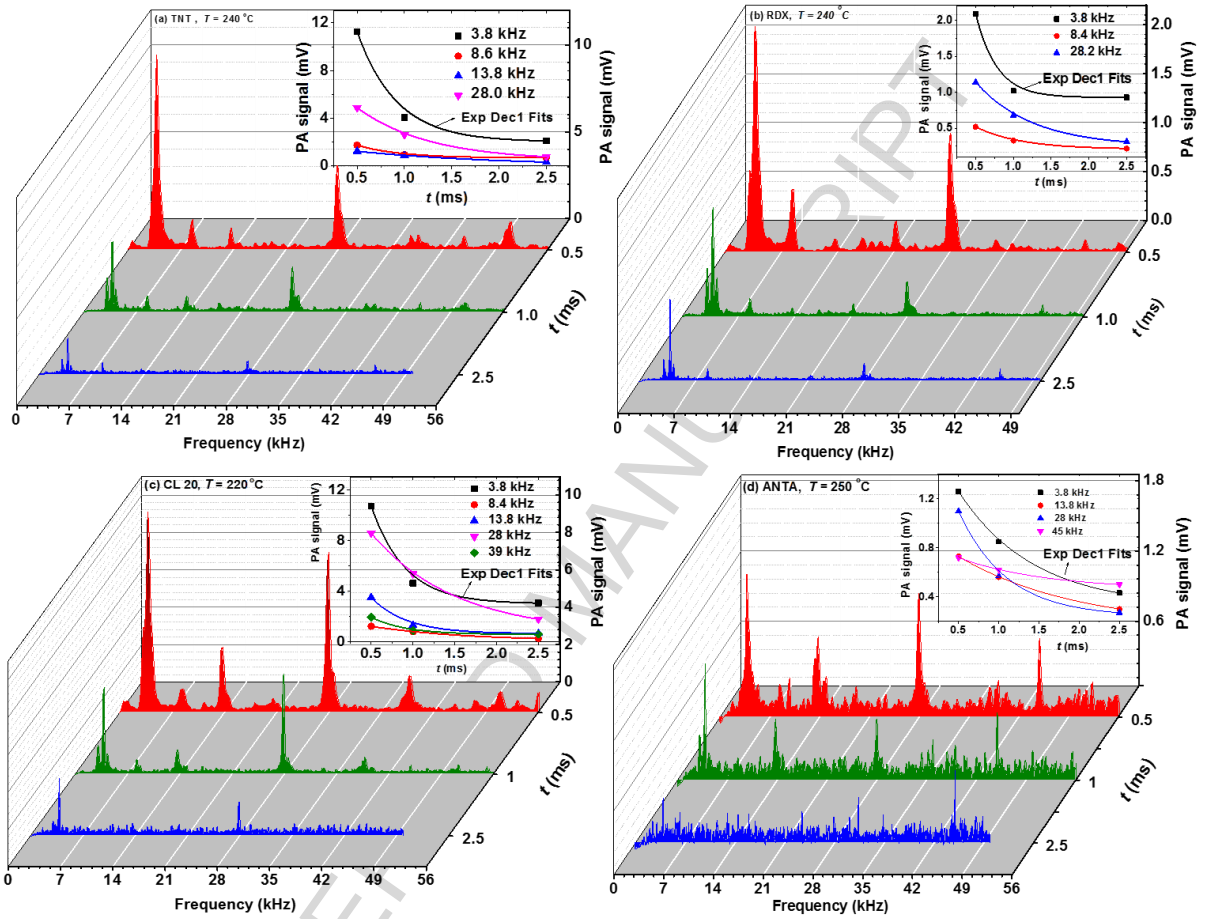

Fig. 8. PA spectra and decay behavior of acoustic modes vs data acquisition time (*t*) for (a) TNT (b) RDX, (c) Cl20, and (d) ANTA.

3.6. Thermal stability of samples based on quality factor

In section 3.2 we have demonstrated the thermal stability of compounds by intensity dependent of PA signal with respect to temperature. In this section, we have tested the stability by considering the quality factor of PA cell (in case of common predominant mode for samples PA spectra) as a function of temperature. It is known that high quality factor can be achieved at high amplification factor. Which shows that the response of PA cell is good enough to record the PA spectra even lower concentration of gaseous molecules.

The quality factor "Q" is defined in terms of the ratio of accumulated energy to the energy loss over one cycle. Physically, it is defined by the ratio of central frequency (ω) to the full width at half maxima ($\Delta\omega_c$) of the corresponding acoustic mode is given by

$$Q = \frac{\omega}{\Delta\omega_c} \tag{1}$$

Fig. 9 show the Lorentz fits of acoustic modes located at ~28 kHz for TNT, RDX, CL20 and ANTA at different temperatures. It is experiential that central frequency of acoustic modes does not show any variation, while full width at half maxima (FWHM) of modes varies as a function of temperature. This evidently indicates that the difference in the concentration of released quantity of gaseous byproducts as a function of temperature. In addition, the intensities of 28 kHz mode for CL20, is higher than other three samples. This is due to modulations in acoustic pressure wave caused by different concentrations of released gaseous molecules. However, the energetic materials possess almost similar acoustic modes due to absorption of 266 nm by all released gaseous fragments irrespective of their quantity in the total gaseous mixture.

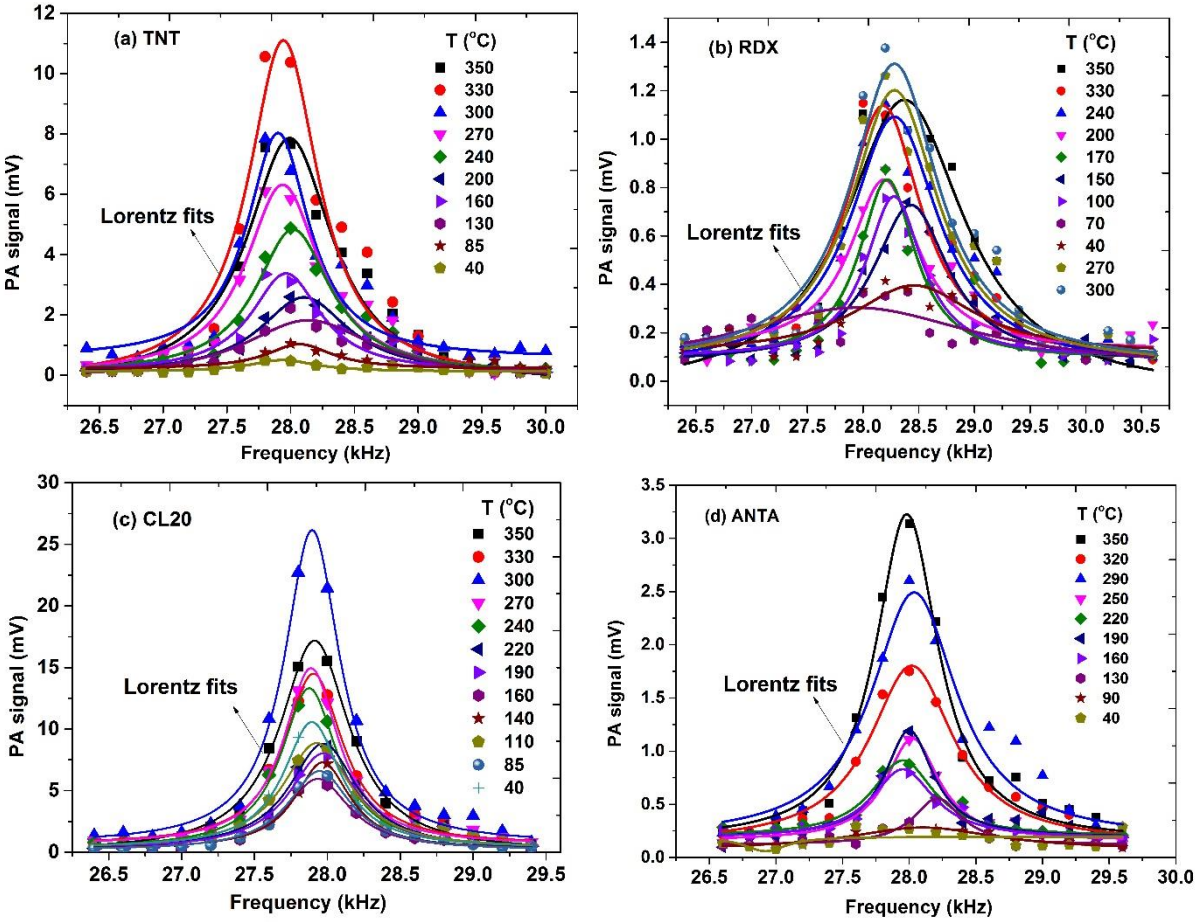

Fig. 9. Lorentz fits of ~28 kHz mode at different temperatures for the samples.

In case of four samples (is shown in Fig. 9), it is clear that the central frequency of ~28 kHz does not vary as a function of temperature. This reveals that the total molecule vapor is contributed for generation of the PA signal using an excitation wavelength λ=266 nm.

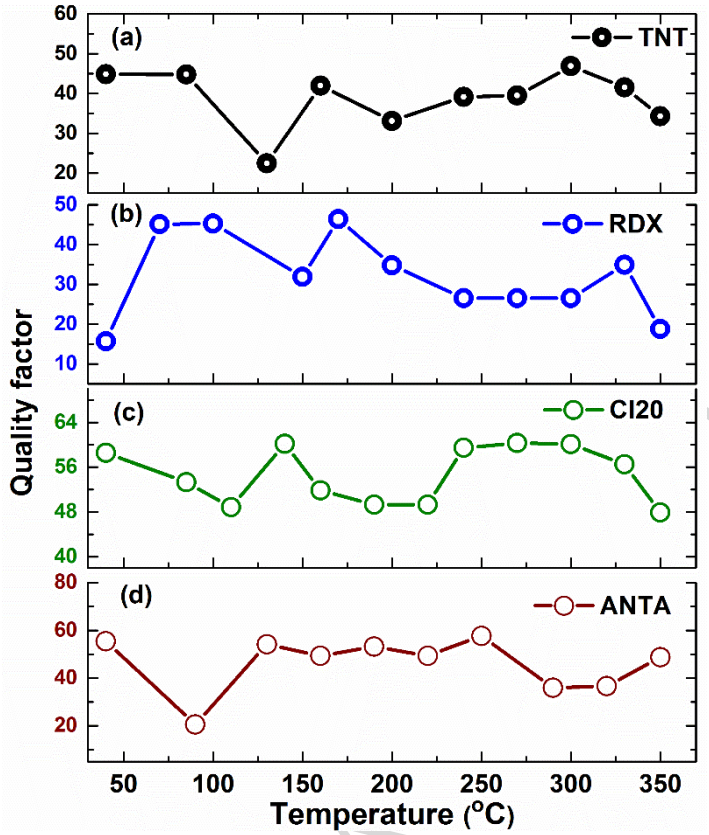

Fig.10. Thermal quality factor of samples at 28 kHz.

Fig. 10(a-d) shows the obtained quality factors for TNT, RDX, CL20, and ANTA, respectively. The highest Q values i.e. 47, 47, 61, and 58 are obtained for TNT, RDX, CL20, and ANTA, at temperatures 300, 170, 270, and 250 °C, respectively. These compounds subsequently release a comparatively higher quantity of gaseous molecules at their melting, decomposition or above the decomposition temperatures than other temperature region. However, the samples possess the similar quality factors at different temperature region (Fig.10). The lower and constant values of quality factors with respect to vapor temperature indicate that the compounds release less quantity of gaseous fragments during the pyrolysis. This indicates the samples are thermally stable as a function of temperature. However, among them, Cl20 possess higher quality factor due to a higher concentration of gaseous molecules within that, which leads to generating the strongest PA signal with the sharp profile (i.e. it has lower FWHM). Therefore, there is a possibility to get the high quality factor 'Q' of PA cavity at these temperatures.

4. Conclusions

We have successfully demonstrated the potential use of the pulsed photoacoustic technique to study the thermal decomposition and stability mechanism of TNT, RDX, CL20, and ANTA, respectively. The thermal PA fingerprint spectra of samples were recorded using 266 nm radiation. The PA signal is generated due to $\pi^* \leftarrow n$ excitation of total molecules vapor. In this report, once again we have demonstrated the potential use of pulsed photoacoustic pyrolysis technique by studying the thermal stability of well-known explosives. The results obtained from PA technique are cross verified with TG-DTA data to confirm the process of thermal decomposition mechanism completes in multiple steps as well as shown their thermal stability. The behavior of acoustic modes were analyzed with respect to incident laser energy, and data acquisition time. In addition, the thermal quality factor is measured to test the stability of explosives.

Acknowledgments: The authors gratefully acknowledge the D.R.D.O., Ministry of Defence, Govt. of India, India, for financial support. Thanks to the Director of ACRHEM, University of Hyderabad for the encouragement,

References

[1] Konda Srinivasa Rao and A.K.Chaudhary, "Development of UV-Vis-THz Laser based Pulsed Photoacoustic Pyrolysis Technique for the Study of Thermal Decomposition, Stability Mechanisms of High Energy Materials," *ILA,Kiran*, no. April, 2017.

[2] J.P. Agrawal, *High Energy Materials*. Wiley, 2010.

[3] Q.-H. Lin *et al.*, "Energetic salts based on 1-amino-1,2,3-triazole and 3-methyl-1-amino-1,2,3-triazole," *J. Mater. Chem.*, vol. 22, no. 2, pp. 666–674, 2012.

[4] A. A. Dippold, D. Izsok, T. M. Klapotke, and C. Pfloger, "Combining the Advantages of Tetrazoles and 1,2,3-Triazoles: 4,5-Bis(tetrazol-5-yl)-1,2,3-triazole, 4,5-Bis(1-hydroxytetrazol-5-yl)-1,2,3-triazole, and their Energetic Derivatives," *Chem. - A Eur. J.*, vol. 22, pp. 1768–1778, 2016.

[5] V. D. Ghule, R. Sarangapani, P. M. Jadhav, and S. P. Tewari, "Theoretical studies on nitrogen rich energetic azoles," *J. Mol. Model.*, vol. 17, no. 6, pp. 1507–1515, 2011.

[6] W. Dehaen and V. A. Bakulev, *Chemistry of 1,2,3-triazoles*. Springer, 2012.

[7] A. Jai Prakash and H. Robert, *Organic Chemistry of Explosives*. Wiley, 2006.

[8] A. S. Kumar, V. D. Ghule, S. Subrahmanyam, and A. K. Sahoo, "Synthesis of thermally stable energetic 1,2,3-triazole derivatives.," *Chemistry*, vol. 19, no. 2, pp. 509–18, Jan. 2013.

[9] A. S. Kumar, N. Kommu, V. D. Ghule, and A. K. Sahoo, "Synthesis of trifluoromethyl-substituted N-aryl-poly-1,2,3-triazole derivatives," *J. Mater. Chem. A*, vol. 2, no. 21, p. 7917, 2014.

[10] N. Kommu, V. D. Ghule, A. S. Kumar, and A. K. Sahoo, "Triazole-substituted nitroarene derivatives: synthesis, characterization, and energetic studies.," *Chem. Asian J.*, vol. 9, no. 1, pp. 166–78, Jan. 2014.

[11] D. Srinivas, V. D. Ghule, K. Muralidharan, and H. D. B. Jenkins, "Tetraanionic nitrogen-rich tetrazole-based energetic salts," *Chem. - An Asian J.*, vol. 8, no. 5, pp. 1023–1028, 2013.

[12] K. S. Rao, F. Yehya, A. K. Chaudhary, A. S. Kumar, and A. K. Sahoo, "Thermal Stability Study of Nitro-rich Triazole Derivatives using Temperature dependent Time resolved Pulsed Photoacoustic (PA) Technique," *J. Anal. Appl. Pyrolysis*, vol. 109, no. 2, pp. 132–139, Jul. 2014.

[13] K. S. Rao, A. K. Chaudhary, F. Yehya, and A. S. Kumar, "Study of acoustic fingerprinting of nitromethane and some triazole derivatives using UV 266nm pulsed photoacoustic pyrolysis technique," *Spectrochim. Acta Part A Mol. Biomol. Spectrosc.*, vol. 147, no. 0, pp. 316–323, Aug. 2015.

[14] K. S. Rao and A. K. Chaudhary, "Study of thermal stability and acoustic fingerprint spectra of phenyl and benzyl triazole derivatives using time-resolved pulsed photoacoustic pyro analysis technique," *Thermochim. Acta*, vol. 614, no. 0, pp. 149–156, 2015.

[15] K. S. Rao and A. K. Chaudhary, "Comparative Study of Ultraviolet Laser-Based Time-Resolved Photoacoustic Fingerprint Spectra and Thermal Decomposition Mechanisms of Energetic 1,2,3-1H-Triazole Derivatives Under Controlled Pyrolysis," *Appl. Spectrosc.*, vol. 71, no. 7, pp. 1–13, 2017.

[16] *Committee on the Review of Existing and Potential Stand-off Explosives Techniques, National Research Council, Washington*. 2004.

[17] A.Croikel, M.Fleischmann, and M. H. and P. J. Hendra, "SURFACE-ENHANCED FOURIER TRANSFORM RAMAN SPECTROSCOPY IN THE NEAR INFRARED," *Chem. Phys. Lett.*, vol. 149, no. 2, pp. 123–127, 1988.

[18] S. M. Angel, L. F. Katz, D. D. Archibald, and D. E. Honigs, "Near-Infrared Surface-Enhanced Raman Spectroscopy. Part II: Copper and Gold Colloids," *Appl. Spectrosc.*, vol. 43, no. 3, pp. 367–372, 1989.

[19] D. B. Chase and B. A. Parkinson, "Surface-Enhanced Raman Spectroscopy in the Near-Infrared," *Appl. Spectrosc.*, vol. 42, no. 7, pp. 1186–1187, 1988.

[20] M. Fleischmann, P. J. Hendra, and A. J. McQuillan, "Raman spectra of pyridine adsorbed at a silver electrode," *Chem. Phys. Lett.*, vol. 26, no. 2, pp. 163–166, 1974.

[21] G. A. West, J. J. Barrett, D. R. Siebert, and K. V. Reddy, "Photoacoustic spectroscopy," *Rev. Sci. Instrum.*, vol. 54, no. 7, pp. 797–817, 1983.

[22] D. W. Ball, "Photoacoustic Spectroscopy," *Spectroscopy*, vol. 21, no. September, pp. 14–16, 2006.

[23] A. Rosencwaig, "Photoacoustic spectroscopy of solids," *Opt. Commun.*, vol. 7, no. 4, pp. 305–308, Apr. 1973.

[24] P. Repond and M. W. Sigrist, "Photoacoustic spectroscopy on trace gases with continuously tunable CO2 laser," *Appl. Opt.*, vol. 35, no. 21, pp. 4065–4085, 1996.

[25] Y. Pinchasov-Grinblat and Z. Dubinsky, "Photoacoustics: A Potent Tool for the Study of Energy Fluxes in Photosynthesis Research," *Artif. Photosynth.*, pp. 257–270, 2012.

[26] A Petzold and R. Niessner, "Novel design of a resonant photoacoustic spectrophone for elemental carbon mass monitoring," *Appl. Phys. Lett.*, vol. 66, no. 10, p. 3,1995.

[27] W. Markus, "Electronic Spectroscopy vibrational, rotational & raman properties," *Photoacoust. Spectrosc. , Appl.*, pp. 1800–1809, 1997.

[28] M. W. Sigrist, A. Bohren, T. Lerber, M. Nägele, and A. Romann, "Environmental Spectroscopy Applications of Photoacoustic," *Anal. Chem.*, vol. 17, pp. 511–514, 2001.

[29] J. B. Kinney and R.H. staley, "Applications of photoacoustic spectroscopy," *Ann.Rev. Mater. Sci.*, vol. 12, pp. 295–321, 1982.

[30] C. S. Sunandana, "Physical applications of photoacoustic spectroscopy," *Phys. status solidi A*, vol. 105, no. 1, pp. 11–43, 1988.

[31] A. Thöny and M. W. Sigrist, "New developments in CO2-laser photoacoustic monitoring of trace gases," *Infrared Phys. Technol.*, vol. 36, no. 2, pp. 585–615, 1995.

[32] W. M. Sigrist, *In Air Monitoring by Spectroscopic Techniques*. New York: John Wiley & Sons, Inc., 1994.

[33] A. Miklós, P. Hess, and Z. Bozóki, "Application of acoustic resonators in photoacoustic trace gas analysis and metrology," *Rev. Sci. Instrum.*, vol. 72, no. 4, pp. 1937–1955, 2001.

[34] V. Slezak, G. Santiago, and A. L. Peuriot, "Photoacoustic detection of NO_2 traces with CW and pulsed green lasers," *Opt. Lasers Eng.*, vol. 40, no. 1–2, pp. 33–41, Jul. 2003.

[35] F. J. M. Harren, G. Cotti, J. Oomens, and S. L. Hekkert, "Photoacoustic Spectroscopy in Trace Gas Monitoring," *Encycl. Anal. Chem.*, pp. 2203–2226, 2000.

[36] S. Schäfer, M. Mashni, J. Sneider, and A. Mikl, "Sensitive detection of methane with a 1 . 65 µ m diode laser by photoacoustic and absorption spectroscopy," *Appl. Phys. B*, vol. 66, pp. 511–516, 1998.

[37] F. Yehya and A. K. Chaudhary, "Time resolved high frequency spectrum of Br_2 molecules using pulsed photoacoustic technique.," *Spectrochim. Acta. A. Mol. Biomol. Spectrosc.*, vol. 115, pp. 544–51, Nov. 2013.

[38] F. Yehya and A. K. Chaudhary, "Study of damping, saturation and surface losses on low level detection of NO2 using time resolved pulsed photo acoustic technique," *Opt. Commun.*, vol. 312, no. 2, pp. 16–22, Feb. 2014.

[39] G. D. Gillispie and A. U. Khan, "The electronic structure of NO2. II. The 2B2← 2A1 and 2B1← 2A1 absorption systems," *J. Chem. Phys.*, vol. 65, no. 5, pp. 1624–1633, 1976.

[40] J. Kalkman and H. W. Van Kesteren, "Relaxation effects and high sensitivity photoacoustic detection of NO 2 with a blue laser diode," *Appl. Phys. B Lasers Opt.*, vol. 90, no. 2, pp. 197–200, 2008.

[41] J. F. Arenas, J. C. Otero, D. Peláez, and J. Soto, "The ground and excited state potential energy surfaces of nitromethane related to its dissociation dynamics after excitation at 193 nm," *J. Chem. Phys.*, vol. 119, no. 15, p. 7814, 2003.

[42] K. S. Rao, D. Ganesh, and A. K. Chaudhary, "Generation of terahertz from $ZnGeP_2$ crystal and its application to record the time-resolved photoacoustic spectra of nitromethane," *Opt. Laser Technol.*, vol. 103, pp. 126–134, 2018.

[43] "The HITRAN 2014 database,online http://www.hitran.com.

[44] F. Yehya, "Designing and Modeling of Efficient Resonant Photo Acoustic Sensors for Spectroscopic Applications," *J. Mod. Phys.*, vol. 2, no. 4, pp. 200–209, 2011.

[45] P. M. Pellegrino, R. G. Polcawich, and S. L. Firebaugh, "Miniature photoacoustic chemical sensor using microelectromechanical structures," in *in Proceedings of SPIE*, 2004, vol. 5416, pp. 42–53.

[46] M. Tavakoli, A. Tavakoli, M. Taheri, and H. Saghafifar, "Design, simulation and structural optimization of a longitudinal acoustic resonator for trace gas detection using laser photoacoustic spectroscopy (LPAS)," *Opt. Laser Technol.*, vol. 42, no. 5, pp. 828–838, 2010.

[47] J. Akhavan, *The Chemistry of Explosives*. The Royal Society of Chemistry, 2011.

Graphical abstract:

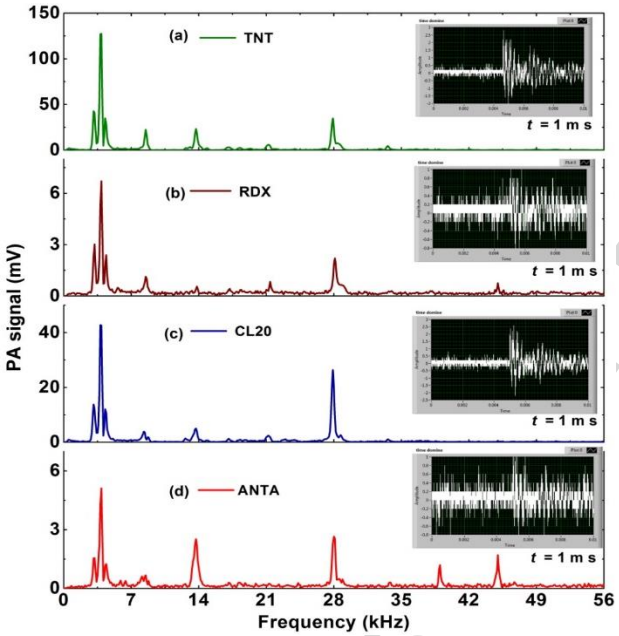

Highlights:

- Demonstartion of UV laser based pulsed photoacoustic spectroscopy to study the thermal stability of some well-known premier explosives such as TNT, RDX, CL20, and ANTA.
- Verification of results obtained from PA spectra and TG-DTA
- Thermal stability study based quality factor "Q".